REPORT DOCUMENTATION PAGE

AFRL-SR-AR-TR-05-

0059

1. REPORT DATE *(DD-MM-YYYY)*	2. REPORT TYPE	3. DATES COVERED *(From - To)*
	Final	29 Sep 2003 - 29 Sep 2004

4. TITLE AND SUBTITLE
Time--Domain Waveforms for Remote Materials Characterization

5a. CONTRACT NUMBER

5b. GRANT NUMBER
F49620-03-1-0441

5c. PROGRAM ELEMENT NUMBER

6. AUTHOR(S)
Douglas R. Denison

5d. PROJECT NUMBER

5e. TASK NUMBER

5f. WORK UNIT NUMBER

7. PERFORMING ORGANIZATION NAME(S) AND ADDRESS(ES)
Georgia Tech Research Institute
505 10th Street, NW
Atlanta, GA 30332-0420

8. PERFORMING ORGANIZATION REPORT NUMBER

9. SPONSORING/MONITORING AGENCY NAME(S) AND ADDRESS(ES)
Air Force Office of Scientific Research
4015 Wilson Blvd
Mail Room 713
Arlington, VA 22203

10. SPONSOR/MONITOR'S ACRONYM(S)
AFOSR

11. SPONSOR/MONITOR'S REPORT NUMBER(S)

12. DISTRIBUTION/AVAILABILITY STATEMENT
Distribution Statement A. Approved for public release; distribution is unlimited.

13. SUPPLEMENTARY NOTES

14. ABSTRACT

This report presents an alternative derivation of the solution given in [1] in terms of the general problem of determining the impulse response of a linear, time-invariant system. The integral equation with chirp excitation and matched filter operator are shown to lead to a Fourier integral representation of the Dirac delta function, which immediately yields the scaling relation shown in [1]. Impoortant practical ramifications of this approach, including the noise properties of the matched filter and the effects of finite-duration chirps are explored. The continuous time integral equation is then discretized in a straight forward manner, and a magic number is presented that allows for the exact recovery of an arbitrart impulse response.

15. SUBJECT TERMS

16. SECURITY CLASSIFICATION OF:			17. LIMITATION OF ABSTRACT	18. NUMBER OF PAGES	19a. NAME OF RESPONSIBLE PERSON
a. REPORT	b. ABSTRACT	c. THIS PAGE			Douglas R. Denison
U	U	U	UU		19b. TELEPHONE NUMBER *(Include area code)*

Final Report for
Time-Domain Waveforms for Remote Materials Characterization

AFOSR Contract # F49620-03-1-0441

Period of Performance: 30 September 2003 – 29 September 2004

Douglas R. Denison
Signature Technology Laboratory
Georgia Tech Research Institute
Atlanta, GA

19 November 2004

1 Summary

The technical report "Multispectral SAR Imaging for Material Identification," ([1]) presents a novel method for directly recovering a time-domain reflection coefficient from the incident and scattered waves. The derivation begins with an integral equation for the reflection coefficient, and proceeds to use a chirp waveform excitation and matched filter operation to find the reflection coefficient to within a scale factor. The basic derivation is then re-cast in discrete form in a linear algebra context, followed by a series of numerical examples.

This report presents an alternative derivation of the solution given in [1] in terms of the general problem of determining the impulse response of a linear, time-invariant system. The integral equation with chirp excitation and matched filter operator are shown to lead to a Fourier integral representation of the Dirac delta function, which immediately yields the scaling relation shown in [1]. Important practical ramifications of this approach, including the noise properties of the matched filter and the effects of finite-duration chirps, are explored. The continuous time integral equation is then discretized in a straightforward manner, and a magic number is presented that allows for the exact recovery of an arbitrary impulse response. This formulation is followed by a brief set of numerical examples that demonstrate the approach. The theoretical portion of the report is concluded with a discussion of antenna effects on chirp waveforms and the use of real (in contrast to complex) chirp waveforms to recover the impulse response.

Time-domain measurements of chirp waveforms were performed as a means to experimentally-validate the analytic approach. We found that the radiated real chirp and associated response were insufficient for use in the complex-chirp based approach developed previously. Comparison of Fourier-transformed data to direct frequency domain measurements further reveals that the chirp measurements suffer from noise that is mitigated in heterodyne systems. In support of program goals, we also measured (in the frequency domain using standard network analyzer techniques) plane wave reflection and transmission for a set of materials of military interest, including cement, drywall, plywood, topsoil, sand, and shingles. Extraction of dielectric constants from these measurements show that many

construction materials have very similar dielectric properties, and that wide-band, low-noise measurements are essential for unique material identification.

2 Chirp Waveform Analysis

2.1 Formulation

Consider a scalar plane wave normally incident upon a material half space, where the time dependent reflection coefficient $R(t)$ defines the ratio of the incident and scattered fields at the interface boundary. The integral equation

$$\psi^s(t) = \int_{-\infty}^{t} R(t-u)\,\psi^i(u)du \tag{1}$$

relates the incident field $\psi^i(t)$ and the scattered (echo) field $\psi^s(t)$ to the unknown reflectivity function $R(t)$. More generally, this expression gives the output of a linear, time-invariant system with impulse response $R(t)$. To explicitly see this characteristic of (1), we can perform a change of variables and re-write the convolution in the more familiar form (explicitly, this is a Fredholm integral equation of the first kind):

$$y(t) = \int_{0}^{\infty} h(s)\,x(t-s)ds = x(t) * h(t), \tag{2}$$

where $\psi^e(t) \rightarrow y(t)$, $\psi(t) \rightarrow x(t)$, and $R(t) \rightarrow h(t)$. We will use this notation throughout as it captures the LTI systems flavor of (1) and separates the solution from any specific physical geometry (such as plane wave reflection from a dielectric slab)[1].

The solution of (2) for an unknown $h(t)$ given the system input $x(t)$ and output $y(t)$ is typically found by transforming the convolution into the frequency domain, where it becomes multiplication:

$$Y(f) = H(f)\,X(f), \tag{3}$$

where $x(t)(y(t), h(t))$ and $X(f)(Y(f), H(f))$ are related by the Fourier transform pair

$$f(t) = \int_{-\infty}^{\infty} F(f)e^{i2\pi ft}\,df \tag{4}$$

$$F(f) = \int_{-\infty}^{\infty} f(t)e^{-i2\pi ft}\,dt. \tag{5}$$

The inverse Fourier transform of the ratio $Y(f)/X(f)$ then yields $h(t)$.

[1] As discussed in our original proposal, knowing $R(t)$ is not in general sufficient to determine material constitutive parameters. In this report, we are principally concerned with implementing algorithms to determine $R(t)$, and thus we prefer the more universal treatment of finding a system impulse response $h(t)$.

2.2 A Closed-Form Solution of Equation (2)

Avoiding the frequency domain altogether, [1] presents a novel solution to the integral equation (2) by first imposing a chirp pulse excitation $x_\gamma(t) = e^{i2\pi f_0 t}\, e^{i\pi\gamma t^2}$ and then applying the matched filter defined as

$$A(t) = \int_{-\infty}^{\infty} x^*(u-t)\, y(u) du. \tag{6}$$

The central result is a simple scaling relation between the matched filter response and the impulse response:

$$h(t) = \gamma A(t). \tag{7}$$

A straightforward derivation of this result begins by noting the additive character of the chirp:

$$x_\gamma(t_1 + t_2) = x_\gamma(t_1) x_\gamma(t_2) e^{i2\pi\gamma t_1 t_2}. \tag{8}$$

Using the chirp waveform excitation ($x(t) = x_\gamma(t)$) and operating on the integral in (2) with the matched filter yields $h(t)$:

$$\begin{aligned}
A(t) &= \int_{-\infty}^{\infty} x^*(u-t) \left\{ \int_0^{\infty} h(s)\, x(u-s) ds \right\} du \\
&= \int_0^{\infty} h(s) \left\{ \int_{-\infty}^{\infty} x^*(u-t)\, x(u-s) du \right\} ds \\
&= \int_0^{\infty} h(s) \left\{ x_\gamma^*(-t) x_\gamma(-s) \int_{-\infty}^{\infty} e^{i2\pi\gamma(t-s)u} du \right\} ds \\
&= \int_0^{\infty} \left\{ x_\gamma^*(-t)\, x_\gamma(-s) \delta(\gamma(t-s)) \right\} ds \\
&= \int_0^{\infty} h(s) \left\{ \frac{1}{\gamma} \delta(s-t) \right\} ds \\
&= \begin{cases} \frac{h(t)}{\gamma}; & 0 < t < \infty \\ 0; & \text{otherwise} \end{cases}.
\end{aligned} \tag{9}$$

2.3 Matched Filter: Unbiased and Minimum Variance Estimator

When combined with the chirp kernel, the matched filter (6) yields the impulse response $h(t)$ to within a scalar factor. Of critical importance to the fidelity of $h(t)$ is the robustness of the matched filter in the presence of noise. We consider in particular the case of noise added to the received signal $y(t) \rightarrow y(t) + n(t)$ (e.g. noise added by receiver electronics), where $n(t)$ is additive white Gaussian noise (AWGN)[2] with zero mean and autocorrelation function $c(\tau) = N\,\delta(\tau)$.

The introduction of noise means the deterministic estimator $h(t)$ (or equivalently $A(t)$) becomes a stochastic estimator $\xi(t) = \hat{h}(t)$, where we use the traditional hat to denote a statistical estimator of a deterministic function. The estimator

$$\xi(t) = \gamma \int_{-\infty}^{\infty} (y(s)_\gamma + n(s))\, x_\gamma^*(s-t)\, ds \tag{10}$$

[2]assumed wide-sense stationary (WSS).

is a random process due to the presence of $n(t)$. We wish to determine if the estimator ξ is unbiased and minimum variance. An unbiased estimator has the property that $E[\xi(t)] = h(t)$; assuming the integrand is uniformly continuous, we can exchange the linear operators $E[-]$ and $\int$, and obtain

$$\begin{aligned} E[\xi(s)] &= \gamma \int_{-\infty}^{\infty} (y_\gamma(t+u_0) + E[n(t)])\, x_\gamma^*(t-s)dt \\ &= \gamma \int_{-\infty}^{\infty} y_\gamma(t+u_0) x_\gamma^*(t-s)dt \\ &= h(s), \end{aligned} \tag{11}$$

where we have used the zero mean nature of the Gaussian process $n(t)$ and the fact that the expectation of a deterministic function is that deterministic function. Since $E[\xi(t)] = h(t)$, the estimator $\xi(t)$ is an unbiased estimator.

For the case of white noise, the estimator is also minimum variance. We shall not prove this fact, which is moderately lengthy. Instead we refer the reader to [2]. The proof in that text for general matched filter architectures applies directly to our scenario. Thus we can conclude that $\xi(t)$ is a pointwise minimum variance, unbiased estimator for the impulse response $h(t)$, and hence asymptotically mean square optimal.

The remaining question is the nature of the estimator noise with respect to the input noise. First, we immediately know that ξ is a wide sense stationary Gaussian random process, since ξ is a linear combination of samples of the wide sense stationary Gaussian random process n. We wish to determine the autocovariance function $D(\tau)$ of ξ with respect to the autocorrelation function of the noise. Note that we deal with the autocovariance function for ξ because ξ is not a zero mean random process. In essence, we are asking how the variance of ξ relates to the variance of n. Then

$$\begin{aligned} D(\tau) &= E\left[\{\xi^*(s) - E[\xi^*(s)]\}\, \{\xi(s+\tau) - E[\xi(s+\tau)]\}\right] \\ &= \gamma^2 E\left[\int_{-\infty}^{\infty} (y_\gamma(q+u_0) + n(q))\, x_\gamma^*(q-s-\tau)dq \right. \\ &\qquad \left. \cdot \int_{-\infty}^{\infty} (y_\gamma^*(t+u_0') + n(t)) x_\gamma(t-s)dt\right] \\ &\qquad -\gamma^2 \int_{-\infty}^{\infty} y_\gamma(q+u_0) x_\gamma^*(q-s-\tau)dq \int_{-\infty}^{\infty} y^*{}_\gamma(t+u_0') x_\gamma(t-s)dt \\ &= \gamma^2 N \int_{-\infty}^{\infty} x_\gamma^*(x-\tau-s) x_\gamma(x-s)dx, \end{aligned} \tag{12}$$

where we have used the fact that $E[n(q)\, n(t)] = \delta(q-t)$ to eliminate one integration.

The expectation is valid for any $s \in (-\infty, \infty)$ due to the wide sense stationarity of the noise, so we choose s=0 yielding the following:

$$D(\tau) = \gamma^2 N \int_{-\infty}^{\infty} x_\gamma^*(v-\tau) x_\gamma(v)\, dv. \tag{13}$$

This gives us the output covariance matrix as a function of the input chirp signal parameters and the noise power N. Note that ξ is not white, due to the power density spectral shaping induced by the matched filter kernel $x(t)$. Thus ξ is a WSS Gaussian random process, with a colored power spectral density.

At first glance one would expect to see the reflection function in the expression for $D(\tau)$. However, the noise is added to $y(t)$ at the output of the system. The noise is not modulated by the reflection function. Hence the noise behavior of the estimator is not influenced by the reflection function, and we have shown the estimator ξ is minimum variance and unbiased in the presence of additive white gaussian noise acting on the received signal $y(t)$. We have also determined the output covariance function $D(\tau)$ of the stochastic estimator $\xi(t)$ for the system parameters γ and the noise power N.

2.4 Finite Duration Chirps

The exact solution (9) to the integral equation requires integrating the chirp product over the entire range $t \in (-\infty, \infty)$. In practice, we cannot operate for an infinite time duration and we are forced to confront the effects of placing a time window of length T around the infinite chirp.

To simplify the mathematics while still providing important insight into finite-duration chirps, consider a delta function impulse response: $h_\delta(t) = \delta(t)$ and the associated matched filter response

$$A_\delta(t) = \int_{-\infty}^{\infty} x^*(u-t) \left\{ \int_0^{\infty} h_\delta(s)\, x(u-s) ds \right\} du. \tag{14}$$

The windowed chirp – defined as $x_\gamma^W(t) = x_\gamma(t), -T/2 < t < T/2;\ 0, \text{otherwise}$ – is used as the source $x(t)$ in (14):

$$\begin{aligned} A_\delta(t) &= \int_{t-T/2}^{t+T/2} x_\gamma^*(u-t) \left\{ \int_0^{\infty} \delta(s)\, x_\gamma(u-s) ds \right\} du \\ &= \int_{t-T/2}^{t+T/2} x_\gamma^*(u-t) x_\gamma(u) du \\ &= \int_{t-T/2}^{t+T/2} x_\gamma^*(-t) e^{i2\pi\gamma ut} du \\ &= x_\gamma^*(-t) \frac{e^{i2\pi\gamma ut}}{\pi\gamma t} \sin(\pi\gamma T t) \\ &= x_\gamma(t) \frac{\sin(\pi\gamma T t)}{\pi\gamma t}. \end{aligned} \tag{15}$$

In the limit as $T \to \infty$, the above result reduces to the expected delta function[3] scaled by γ; for finite T, the result is a smeared version of the delta function (scaled by the chirp waveform), represented by the sinc function. This solution agrees with the general observation that finite time windows perform a smearing on a response to a linear, time-invariant system.

[3] $\lim_{T\to\infty} \frac{\sin(\pi\gamma T t)}{\pi\gamma t} = \pi\delta(\pi\gamma t) = \frac{\delta(t)}{\gamma}$

2.5 Numerical Implementation

2.5.1 Formulation

The numerical evaluation of the matched filter response (9) is most easily accomplished by reconsidering the integral equation (2) in its discrete form. Using this approach, we assume that the finite-duration chirp signal is not a windowed version of a chirp; rather, it is one period of a periodically-replicated function. As such, we will show that for particular choices of chirp parameter and period duration, we can exactly recover the impulse response via the chirp excitation/matched filter operation.

Consider uniformly discretized time samples such that $t_n = n\Delta t, n = \ldots, -2, -1, 0, 1, 2, \ldots$. The discrete-time form of the system response becomes

$$y(t_n) = \sum_{t_r} h(t_r)x(t_n - t_r)\Delta t. \tag{16}$$

The matched filter takes the form

$$A(t_n) = \sum_{t_s} x^*(t_s - t_n)y(t_s). \tag{17}$$

As before in the continuous case, we have

$$\begin{aligned} A(t_n) &= \sum_{t_r} h(t_r) \left\{ \sum_{t_s} x_\gamma^*(t_s - t_n)x_\gamma(t_s - t_r) \right\} \Delta t \Delta t \\ &= \sum_{t_r} h(t_r) \left\{ x_\gamma^*(-t_n)x(-t_r) \sum_{t_s} e^{i2\pi\gamma(t_n - t_r)t_s} \right\} \Delta t \Delta t. \end{aligned} \tag{18}$$

Let $t_s = \{[-N : N]\Delta t\}$ and recall that

$$\sum_{s=-N}^{N} e^{i\alpha s} = \frac{\sin[(2N+1)\alpha/2]}{\sin(\alpha/2)} = (2N+1)\left[\delta_{t_n t_r} + O\left(\frac{1}{2N+1}\right)\right], \tag{19}$$

where $\delta_{t_n t_r}$ is the Kronecker delta function. Then

$$\begin{aligned} A(t_n) &\approx \sum_{t_r} h(t_r) \left\{ x_\gamma^*(-t_n)x_\gamma(-t_r)(2N+1)\delta_{t_n t_r} \right\} \Delta t \Delta t \\ &\approx \begin{cases} h(t_n)(2N+1)\Delta t \Delta t & \text{if} \quad t_r \in t_n \\ 0 \quad \text{otherwise} \end{cases} . \end{aligned} \tag{20}$$

An important contrast between this result and the results presented in [1] is the fact that we have not specified the support of $h(t)$. For practical purposes, we assume that $h(t) = 0$ for t outside the range $[-N\Delta t : N\Delta t]$ since in actuality we can never know the support of $h(t)$ and must choose chirps long enough to at least capture $h(t)$.

The Magic Number

Re-examining the steps that lead to (20), let us reconsider the original series (18). We assume that all discrete time values t_s, t_r, and t_n are discretized with equal Δt so $t_n - t_r = m\Delta t$, where $m = \ldots, -2, -1, 0, 1, 2, \ldots$. Then we can write the inner nested sum in (18) as

$$\mathcal{S} = \sum_{s=-N}^{N} e^{i2\pi\gamma m\Delta t \cdot s\Delta t} = \sum_{s=-N}^{N} e^{i2\pi\gamma m s\Delta t^2}. \tag{21}$$

Suppose that we choose Δt to be the *magic number* $(N\gamma)^{-\frac{1}{2}}$, then

$$\begin{aligned} \mathcal{S} &= \sum_{s=-N}^{N} e^{i2\pi\frac{m}{N}s} \\ &= \begin{cases} 2N+1; & m = 0 \\ 0; & \text{otherwise} \end{cases} . \end{aligned} \tag{22}$$

Numerically, the magic number provides for complete cancellation of the set of vectors $e^{i\alpha s}$ in the complex plane by setting α equal to an integer number of intervals in the unit circle. This property is related to the Nyquist sampling rate, where there are exactly two samples per 2π radians. We can see this explicitly by considering the time-dependent frequency of the chirp, $f(t) = f_0 + \frac{\gamma}{2}t$. The highest frequency of the signal occurs when t is a maximum: $t = N\Delta t$. Setting $f_0 = 0$ (without loss of generality, as we can always mix down the harmonic component of the signal) and using the magic number for Δt we find the maximum frequency is

$$f_{\max} = \frac{\gamma}{2}N\Delta t = \frac{1}{2}\frac{1}{\Delta t^2}\Delta t = \frac{1}{2\Delta t}. \tag{23}$$

Recalling the Nyquist rate gives the highest frequency that can be sampled with a period of Δt as $f_{\text{nyq}} = \frac{1}{2\Delta t}$, we see that $f_{\max}$ is identically the Nyquist frequency when Δt is the magic number.

Our constraint that $f_0 = 0$ is related to the Zak transform analysis given in a subsequent Progress Report [3] by the authors of [1]. Leaving the detailed derivation to [3], the Zak space representation of the chirp begins with a discretized waveform of duration T sampled at N uniform points, where the Zak space is defined by dimension $L \times K$, with measures $N = LK$ and $M = K/L$. Discretizing the chirp yields parameters $a = \gamma\frac{T^2}{K^2}$ (discrete chirp rate) and $b = f_0\frac{T}{K}$ (discrete carrier frequency). The authors show that a chirp can be represented as a line (or set of lines) in Zak space provided that $x(N) = 1$, $aM \in Z$, and aM^2 and $2bM$ are either both odd or both even integers. These parameter constraints result from requiring modulo N periodization of the sampled chirp; as noted above, the magic number arises from a similar periodization (i.e. perfect cancellation of terms over the series).

To see the relation between the magic number derivation and [3]'s result for the Zak space condition, consider the impact of the parameter constraints on the Nyquist frequency. The quantity

$$aM = \gamma\frac{T^2}{K^2} \cdot \frac{K}{L} = \gamma\frac{T^2}{N} = \gamma T\Delta t_{\text{samp}} \in Z \tag{24}$$

must be greater than or equal to 1 since it is a positive integer. Conversely, the Nyquist frequency of the chirp (following (23) with $f_0 \neq 0$) gives

$$\Delta t_{\text{nyq}} = \frac{1}{\gamma T + 2f_0}. \tag{25}$$

In order for these two conditions to hold (that is, for $\Delta t_{\text{samp}} \leq \Delta t_{\text{nyq}}$), f_0 must be identically zero.

The implication here is two-fold: we have shown that the magic number derived above and the Zak space condition from [3] share a common analytic underpinning and (more importantly) we see that the chirp can never be (ideally) sampled to meet the Nyquist criterion if the carrier frequency f_0 is > 0. In practice, f_0 can be made zero by down-converting the baseband signal prior to discretization, or it may prove that the aliasing introduced by $f_0 > 0$ occurs at frequencies above the frequency of interest.

2.6 Numerical Examples

2.6.1 Simple Response

In the following figures, we show the discrete-time recovery of two simple, closed-form impulse responses via (20). The impulse responses are a delta function at $t = 4\Delta t$ (Figures 1 and 2), and a Gaussian response $h(t) = e^{-[(t-0.1)/0.035]^2}$ (Figures 3 and 4). In both cases we have used the magic number with $\gamma = 10, N = 500, dt = 0.01$ and $f_0 = 0$, and we see that the real part of the impulse response matches the given (real) response, while the imaginary part is numerically zero. Figure 5 shows the result of recovering the impulse response $\delta(t - 4\Delta t)$ with arbitrary parameters that do not meet the magic number criteria; comparing these results to Figure 1, we see that the imaginary part becomes appreciable, as do the ripples around the peak of the delta function. These ripples follow mathematically directly from the results in (20), where we have an error term of $O(2N + 1)$.

2.6.2 Dielectric Slab Example

A more challenging example is presented by determining the reflection coefficient from a dielectric slab, which is a realistic physical geometry with extensive time/frequency structure due to ringing of resonant modes in the slab. Figure 6 shows the frequency domain reflection coefficient for a plane wave incident on an infinite dielectric slab with thickness 0.508m and dielectric constant $\epsilon_r = 8.0$. The closed-form solution is found from the standard frequency domain technique of matching boundary conditions at the slab interfaces; the chirp solution is found from the matched filter response (20). The magic number for Δt is used, and the chirp parameters are $\gamma = 0.017$ GHz/ns, $f_0 = 0$, and $N = 1024$. As the figure shows, the agreement between the different techniques is excellent, demonstrating that with the magic number, we can numerically implement ideal reconstruction of the impulse response.

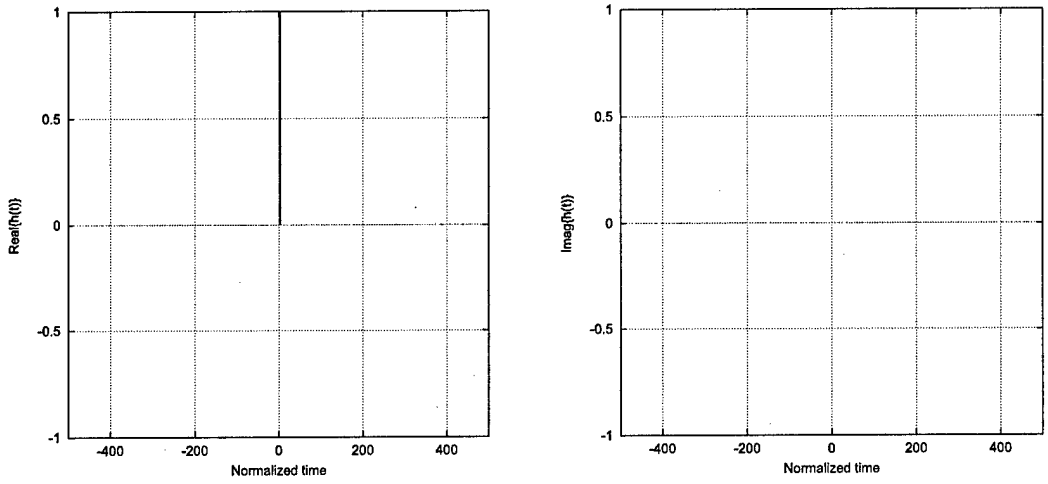

(a) Real (b) Imaginary

Figure 1: Impulse response computed from the matched filter response with $h(t) = \delta(t - 4\Delta t), \gamma = 10, f_0 = 0, \Delta t = 0.01, N = 500$.

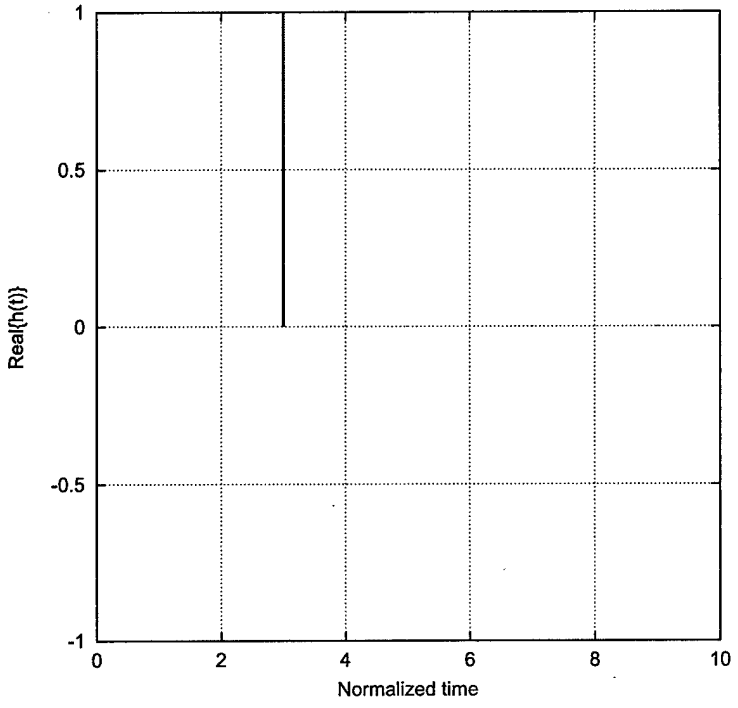

Figure 2: Detail of the real part of the impulse response shown in Figure 1.

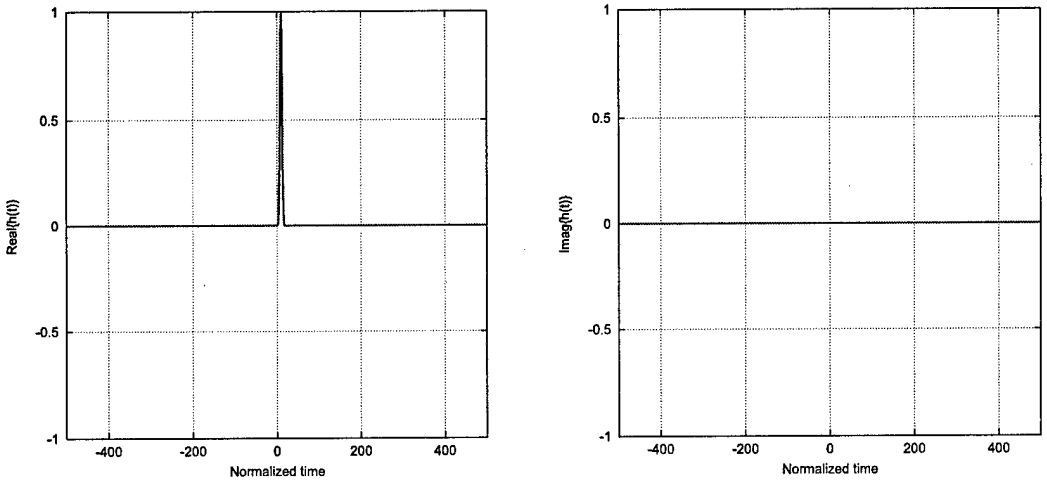

(a) Real (b) Imaginary

Figure 3: Impulse response computed from the matched filter response with $h(t) = e^{-[(t-0.1)/0.035]^2}, \gamma = 10, f_0 = 0, \Delta t = 0.01, N = 500$.

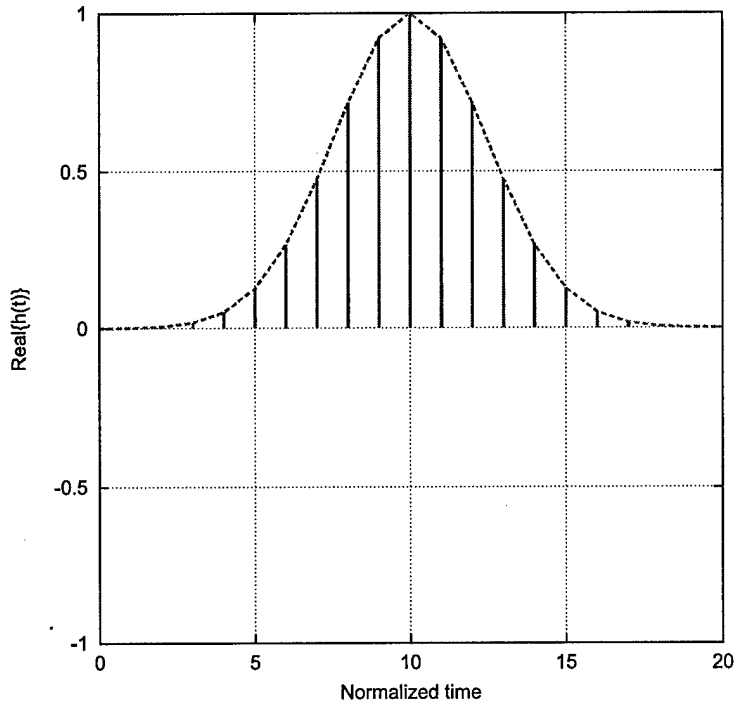

Figure 4: Detail of the real part of the impulse response shown in Figure 3.

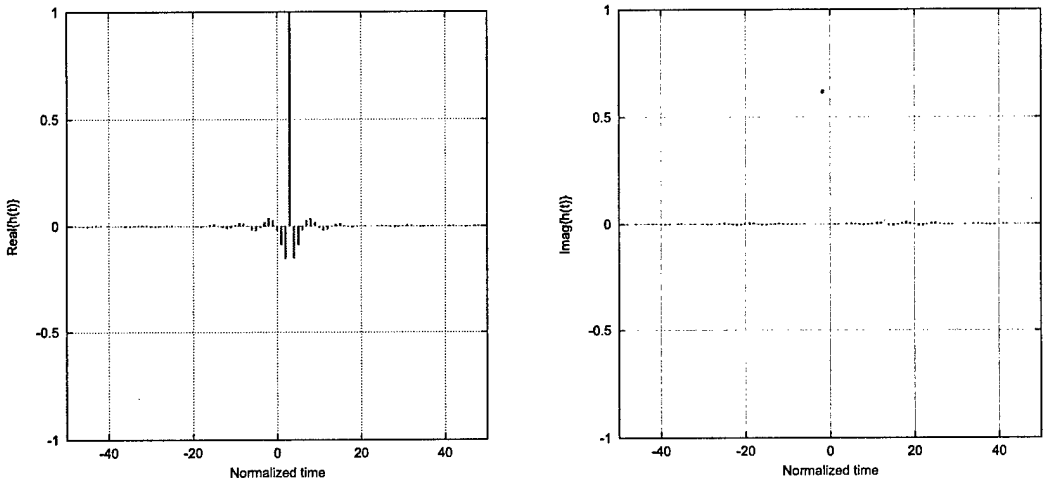

(a) Real (b) Imaginary

Figure 5: Impulse response computed from the matched filter response with $h(t) = \delta(t - 4\Delta t), \gamma = 10, f_0 = 0, \Delta t = 0.01, N = 850$.

2.7 Practical Considerations: Antenna Effects and Real Chirps

2.7.1 Antenna Effects

In a Synthetic Aperture Radar (SAR) system (for which this approach is proposed for materials identification), a critical effect is the dispersion caused by the transmitting/receiving system. At the 29 October, 2003, Technical Interchange Meeting, we presented an analysis of chirp pulse distortion due to measured dispersion in a two-antenna transmission system. We noted that the echo waveform is not only a function of the reflectivity, but also of the transfer characteristics of the antenna system. In the frequency domain, we write this explicitly as

$$\Psi^s(f) = \Psi^i(f)R(f)H(f), \tag{26}$$

where $\Psi(f)$ is the Fourier transform of $\psi(t)$, $R(f)$ is the frequency-domain reflectivity (Fourier transform of $R(t)$), and $H(f)$ is the antenna system response.

A reflectivity derived from the echo in such a system will be a distorted $R'(f) = H(f)R(f)$ (or $R'(t)$) that includes the antenna response; Figure 7 shows the measured frequency response $H(f)$ for a pair of horn antennas separated by 1 m. Figure 8 shows the time-domain distortion of a chirp with $f_0 = 1$ GHz and $\gamma = 0.01$ GHz/ns due to the two-antenna transfer function, and Figure 9 gives the chirp's frequency spectrum. In this case of a chirp with a narrow spectrum, the distortion caused by the antenna is not significant since $H(f) \approx$ constant over any given narrow frequency band. The chirp parameter and thus frequency content are increased for the chirp shown in Figure 10 (frequency in Figure 11), and the distortion of the chirp is much more pronounced. Here we clearly see that antenna effects must be compensated for (through e.g. prior system calibration) to accurately reconstruct the impulse response.

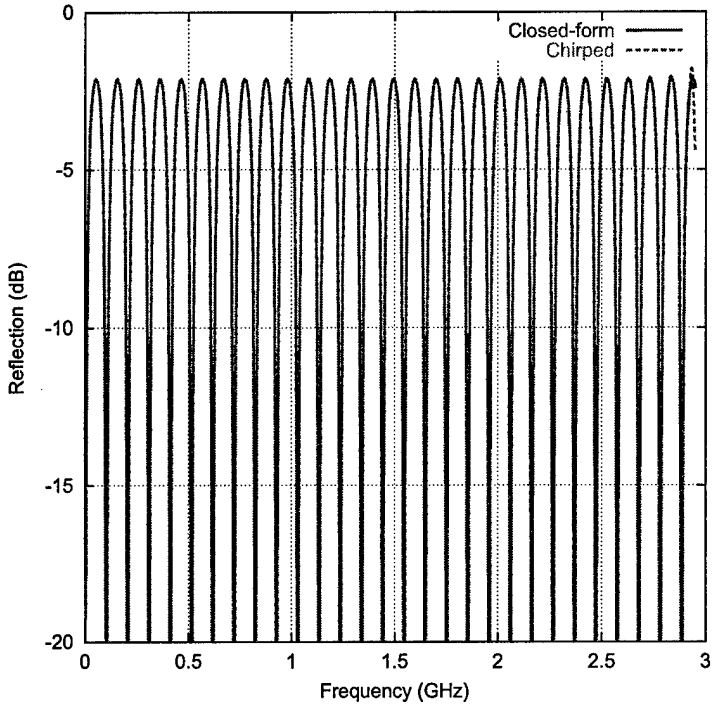

Figure 6: Computed reflection coefficient for a dielectric slab with thickness $t = 0.508$m and $\epsilon_r = 8.0$. .The solid line is based on a direct, closed-form frequency domain calculation of the reflection coefficient. The dashed line results from the matched filter/chirp solution with $\gamma = 0.017$ GHz/ns, $f_0 = 0$, and $N = 1024$. The magic number for Δt was used.

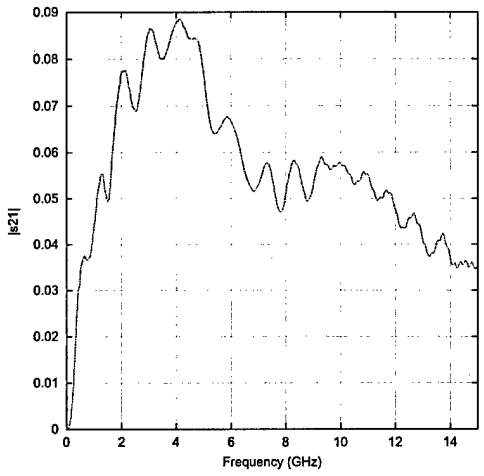

Figure 7: Magnitude of the two horn antenna system transfer function used to compute antenna-induced chirp distortion shown in Figures 8 and 10.

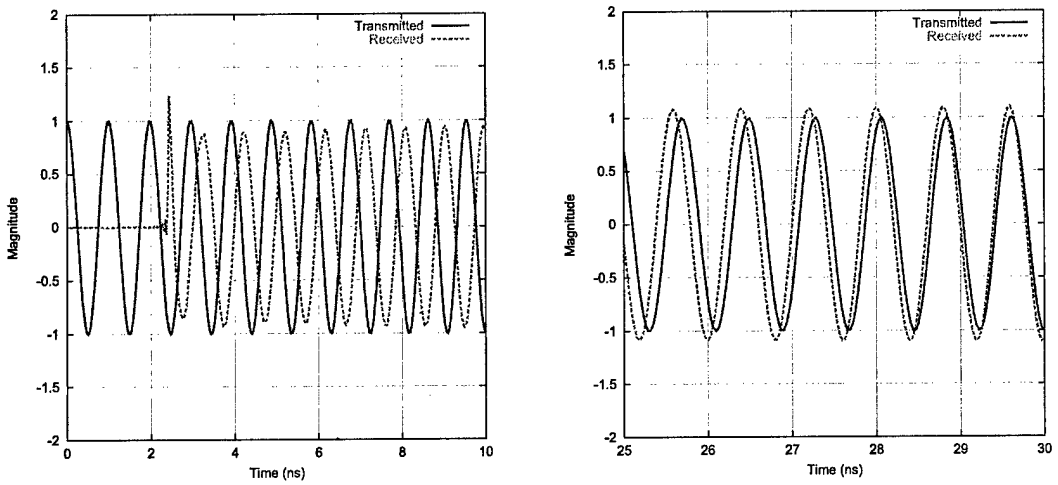

(a) Early Time

(b) Late Time

Figure 8: Chirp waveform numerically propagated through two antenna system. Chirp parameters are $\gamma = 0.01$ GHz/ns and $f_0 = 1$ GHz.

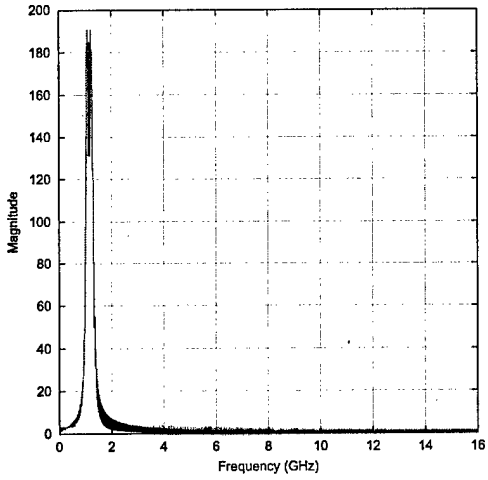

Figure 9: Spectrum of transmitted chirp shown in Figure 8. Chirp parameters are $\gamma = 0.01$ GHz/ns and $f_0 = 1$ GHz.

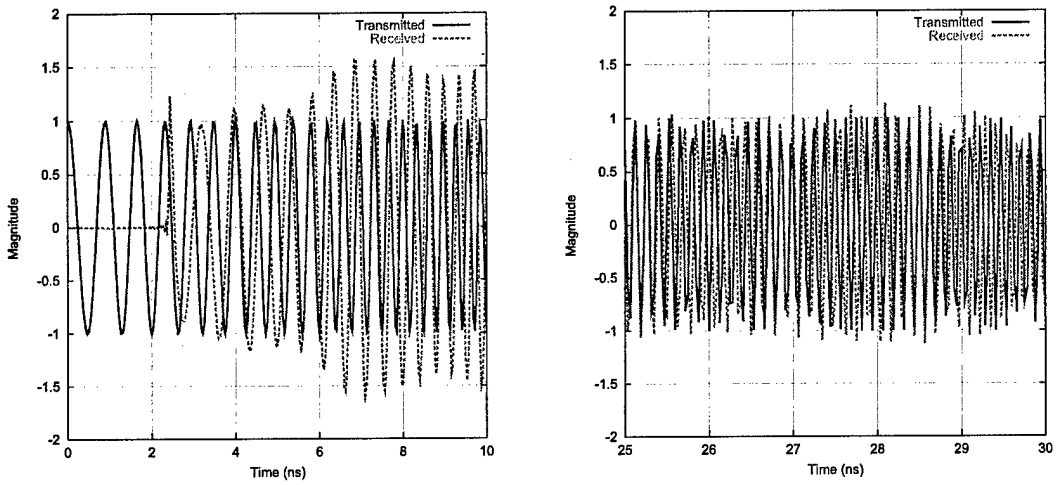

(a) Early Time

(b) Late Time

Figure 10: Chirp waveform numerically propagated through two antenna system. Chirp parameters are $\gamma = 0.25$ GHz/ns and $f_0 = 1$ GHz.

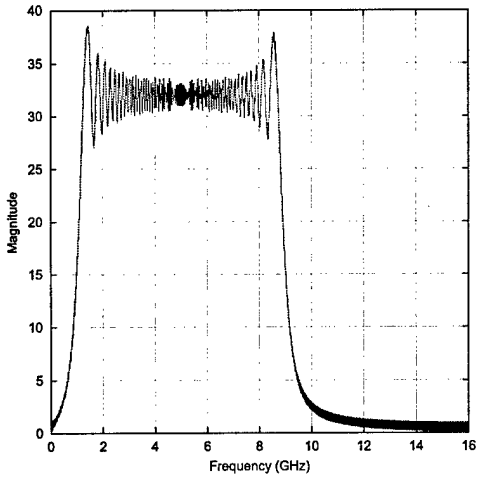

Figure 11: Spectrum of transmitted chirp shown in Figure 10. Chirp parameters are $\gamma = 0.25$ GHz/ns and $f_0 = 1$ GHz.

2.7.2 Real Chirps

The integral equation solution given in Section 2.1 requires a complex chirp excitation, and its reliance on chirp products (namely, the additive property and the matched filter integrand) precludes decomposing the solution into real and imaginary parts. In practice, producing complex chirp waveforms for radiation is difficult. Although the complex chirp can be written as $x_r(t) + ix_i(t)$, the quadratic time-dependence does not allow for a simple scaling or shift relation between the quadrature terms. In the above chirp distortion examples, we drove the antenna system with the real part of the chirp ($x(t) = \Re\{x_\gamma(t)\} = \cos(2\pi f_0 t + \pi\gamma t^2)$) to accurately represent a practical implementation. In order to apply the system response solution with a complex chirp excitation, we must be able to recover the imaginary part of the chirp from the real part.

Assume that $h(t)$ real and that $x(t) = x_r(t)+ix_i(t)$ is a known, prescribed input waveform. Then

$$\begin{aligned} y_r(t) = h(t) * x_r(t) &\Leftrightarrow Y_r(f) = H(f)X_r(f) \\ y_i(t) = h(t) * x_i(t) &\Leftrightarrow Y_i(f) = H(f)X_i(f). \end{aligned} \tag{27}$$
(28)

If we are able to only measure $y_r(t)$, we can recover $y_i(t)$ according to

$$Y_i(f) = \frac{X_i(f)}{X_r(f)} Y_r(f) \Leftrightarrow y_i(t) = \mathcal{F}^{-1}\left\{\frac{X_i(f)}{X_r(f)}\right\} * y_r(t). \tag{29}$$

Since $x(t)$ is the known excitation, we can in principle pre-compute $X(f)$ (more precisely, the ratio $\frac{X_i(f)}{X_r(f)}$) and use it to synthesize $y_i(t)$ from $y_r(t)$.

The Fourier transform for the chirp is derived as follows. Consider the Fresnel integral whose solution is generated by the Cornu spiral evaluated at $\pm\infty$:

$$\int_{-\infty}^{\infty} e^{j\beta s^2}\, ds = \sqrt{\frac{\pi}{2\beta}}\,(1+j). \tag{30}$$

The Fourier transform (using the conventions established in (4)) of the real part of the chirp is

$$\begin{aligned} X_r(f) &= \int_{-\infty}^{\infty} \cos(\pi\gamma t^2)\cos(2\pi f t)\, dt \\ &= \Re\left[\int_{-\infty}^{\infty} e^{j\pi\gamma t^2}\cos(2\pi f t)\, dt\right] \\ &= \frac{1}{2}\Re\left[\int_{-\infty}^{\infty} e^{j\pi\gamma t^2} e^{2\pi j f t} dt\right] + \frac{1}{2}\Re\left[\int_{-\infty}^{\infty} e^{j\pi\gamma t^2} e^{-2\pi j f t} dt\right], \end{aligned} \tag{31}$$

where we have (without loss of generality) set $f_0 = 0$ and exploited the resulting evenness of the chirp function. Completing the square in the exponent terms and using the Fresnel integral result gives

$$X_r(f) = \frac{1}{\sqrt{2\gamma}}\left(\cos\left(\frac{\pi f^2}{\gamma}\right) + \sin\left(\frac{\pi f^2}{\gamma}\right)\right). \tag{32}$$

A similar procedure is used to find $X_i(f)$:

$$X_i(f) = \frac{1}{\sqrt{2\gamma}} \left(\cos\left(\frac{\pi f^2}{\gamma}\right) - \sin\left(\frac{\pi f^2}{\gamma}\right) \right). \tag{33}$$

Although we have derived the Fourier transform of the complex chirp, the ratio required to implement (29) is problematic. The existence of f^2 terms in the denominator ($X_r(f)$) creates an infinite density of unremovable singularities along the real f axis.

3 Measurements

3.1 Time-Domain Chirp Waveform Measurements

We performed a series of chirp waveform measurements using a sweep generator source and a digital oscilloscope receiver (Figure 12) with the goal of implementing (20) for measured data on a number of systems. These systems included a direct throughput, a pair of horn antennas, and a fixed length of transmission line; the chirp waveform in all cases was swept from an initial frequency of 250 MHz to 1250 MHz (a 5:1 bandwidth) over a time of 10 ms. These parameters yield a chirp waveform with $f_0 = 0.25$ GHz and $\gamma = 2 \times 10^{-7}$ GHz/ns. The resulting data sets are quite large due to the 2.5 GS/s sampling rate over a 20 ms measurement duration; displays of the time-domain data are too dense to read. We developed a technique for looking at the data that determines the center frequency within short (compared to γ) time windows to reveal how the frequency increases with time. Figure 13 shows frequency as a function of time, with a time window of 4096 samples (1.64 μs). As the figure shows, the chirp waveform continuously increases from 250 MHz to 1250 MHz, demonstrating that the RF generator does indeed produce a continuous chirped waveform.

These measurements were performed before the analysis presented in Section 2.7.2 was complete, and that result shows that the measurement of real chirp excitation of the system is insufficient to recover the system response. Furthermore, the measured chirp, while real, does not easily map to the real or imaginary part of the complex chirp $x_\gamma(t)$; that is, the excitation has the form $x(t) = \cos(2\pi f_0 t + \pi\gamma t^2 + \phi)$, where ϕ is some (generally unknown) phase offset. Taken together, these effects indicate that measured waveforms do not easily adapt to the theoretical analysis presented in Section 2.

Independent of the chirp solution to the integral equation (2), the time-domain measurements also suffer from noise. Material and systems measurements are typically performed in the frequency domain, where heterodyne mixing affords signal to noise ratios in the < -60 dB range. The effects of noise on the time domain measurements are clearly shown in Figure 14, where we have computed the frequency-domain transfer characteristic for a pair of horn antennas from the time-domain chirp measurements. Figure 15 shows the influence of small time offsets on the ability to accurately recover phase. The straight-line nature of the phase difference indicates that the shape of the time-domain reconstructed phase is the same as the shape of the measured frequency-domain phase, but the magnitude of the slope indicates the differing phase rolls due to different (apparent) time delays.

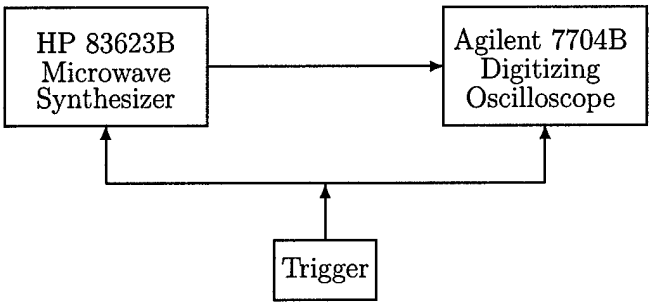

Figure 12: Configuration to directly measure chirp waveform generated by the sweep microwave source.

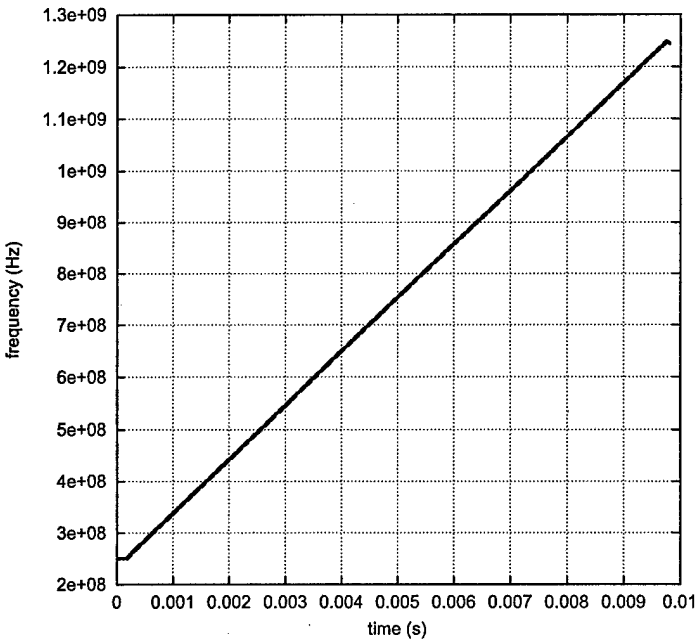

Figure 13: Measured chirp frequency as a function of time. Frequency is determined by taking a moving window average through the data with a window duration of 1.6μs. Total measurement time was 20 ms.

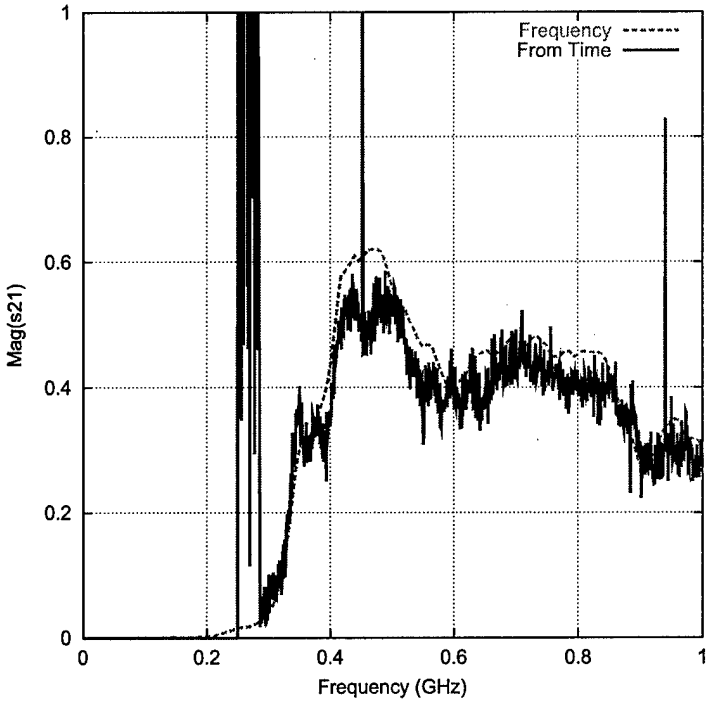

Figure 14: Magnitude of the measured transfer characteristic of a pair of horn antennas spaced 10" apart. The dashed line is a direct frequency measurement of the transfer function (s21), and the solid line is derived from the ratio of the Fourier transforms of the time-domain chirp waveform data.

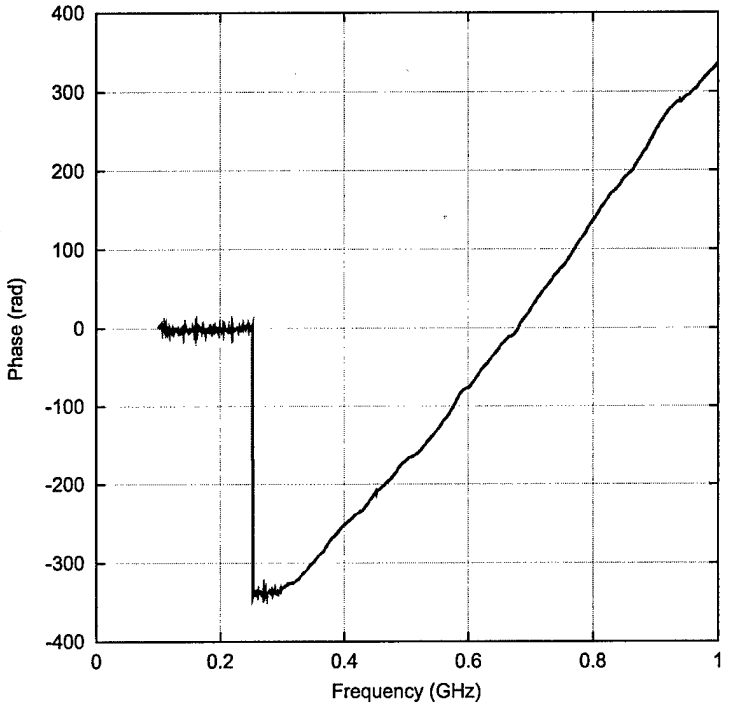

Figure 15: Difference in frequency-domain measured and time-domain derived transfer function (s21) phases for a pair of horn antennas spaced 10" apart.

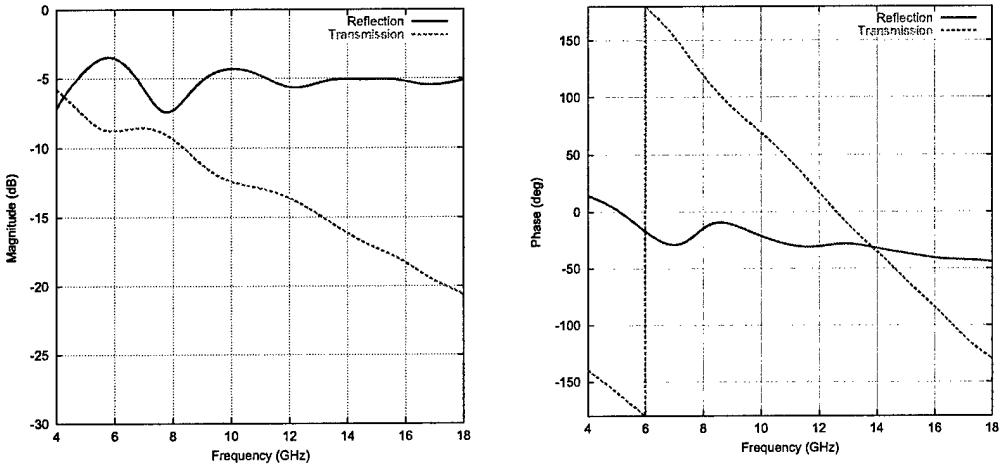

(a) Magnitude

(b) Phase

Figure 16: Measured reflection and transmission coefficient magnitudes and phases for 0.5" thick concrete backer board.

3.2 Materials of Military Interest

Following the discussions at the October TIM, we performed measurements on a subset of materials of military interest. They include: cement backerboard, drywall, topsoil, sand, asphalt roof shingles, and plywood. In all cases, the materials were measured on our focused beam lens system, which creates a field with a uniform (plane-wave-like) phase and Gaussian amplitude taper (to avoid sample edge effects) at the sample surface that approximates plane wave illumination. Measurements were performed over the 4 – 18 GHz frequency range and are calibrated against through and reflection standards.

Representative results from the measurements are demonstrated by the cement backerboard reflection and transmission coefficients (Figure 16). These measurements are then used to extract the permittivity of the material assuming $\mu_r = 1$; the resulting complex permittivity is shown in Figure 17. The measured properties of the remaining materials are summarized in Figures 18 through 25; we were not able to reliably extract dielectric constants for the shingles and topsoil due to high absorption (water content) in the materials.

These measurements further demonstrate the difficulties associated with using the chirp waveform analysis for materials identification. For instance, the method used to derive the dielectric constant from the measurements requires knowledge of both the reflection and transmission coefficients – information that is not provided by the matched filter response formulation. Furthermore, an interesting property of these materials is that they have relatively constant dielectric properties over the range of microwave frequencies from 4 – 18 GHz, and three of the materials (drywall, sand, and plywood) have very similar values of dielectric constant. Taken together, these characteristics indicate the need for low noise, wide bandwidth material measurements that are difficult to achieve with a chirped waveform.

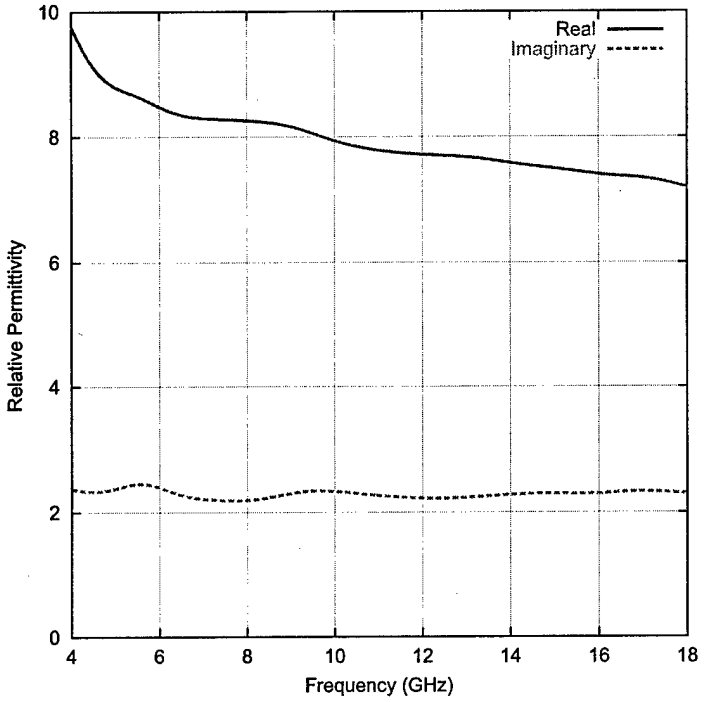

Figure 17: Complex permittivity for concrete backer board extracted from measured data.

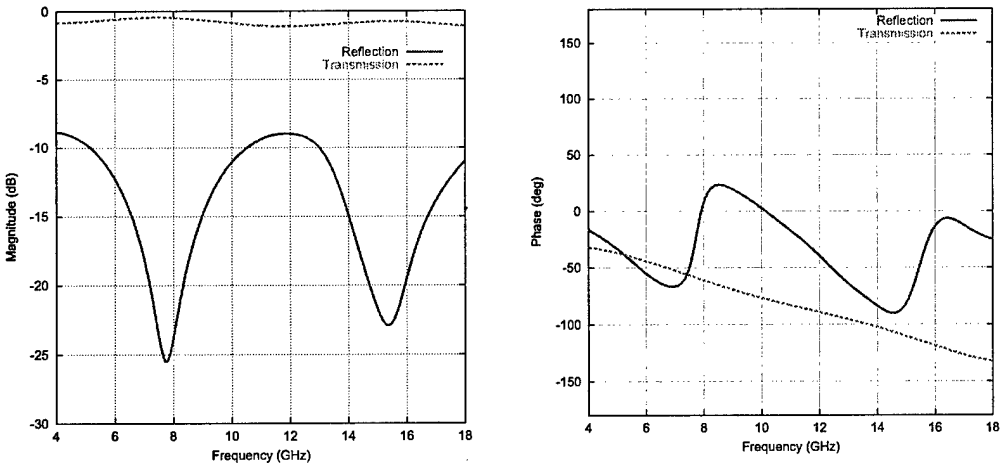

(a) Magnitude

(b) Phase

Figure 18: Measured reflection and transmission coefficient magnitudes and phases for 0.5" thick drywall.

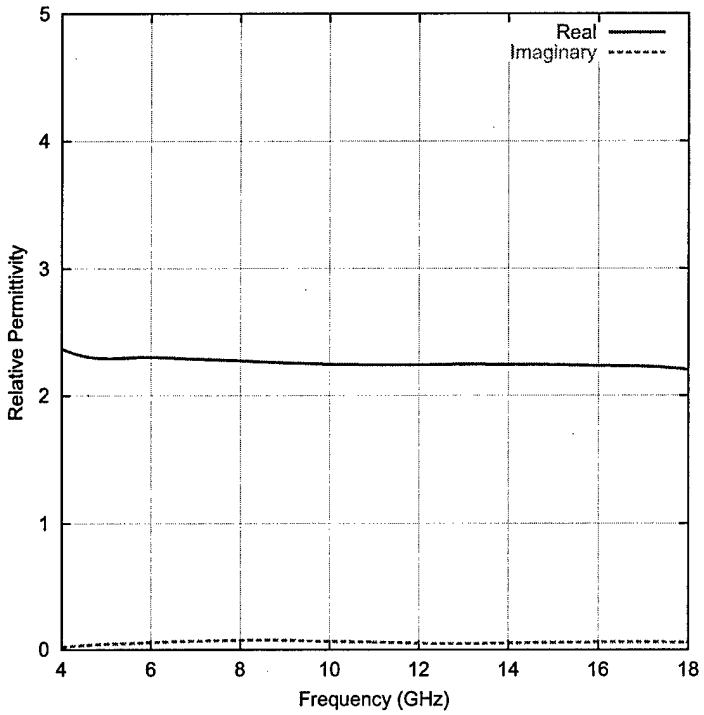

Figure 19: Complex permittivity for drywall extracted from measured data.

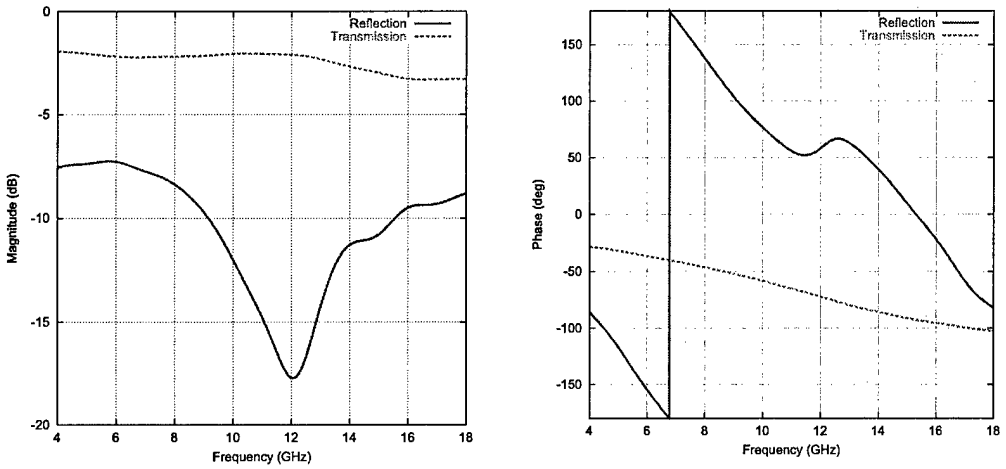

(a) Magnitude

(b) Phase

Figure 20: Measured reflection and transmission coefficient magnitudes and phases for 0.28" thick plywood.

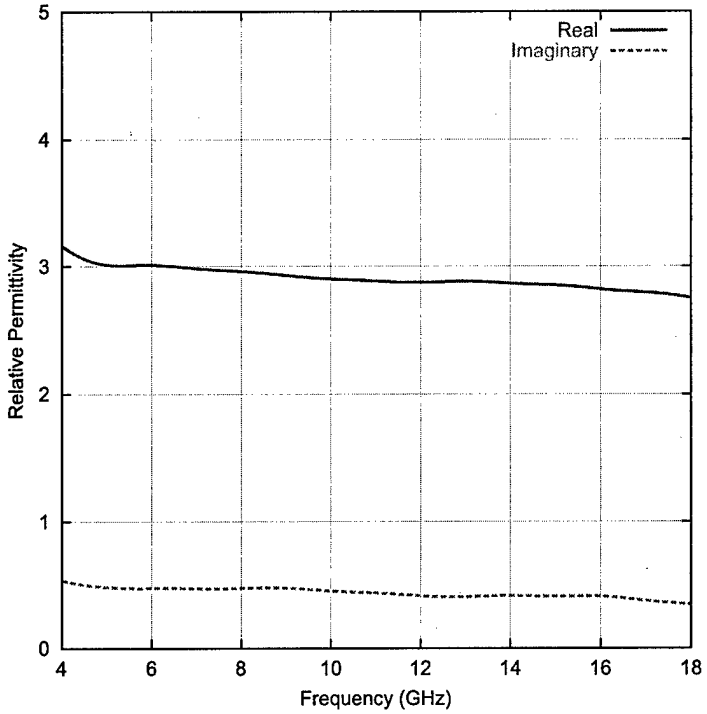

Figure 21: Complex permittivity for plywood extracted from measured data.

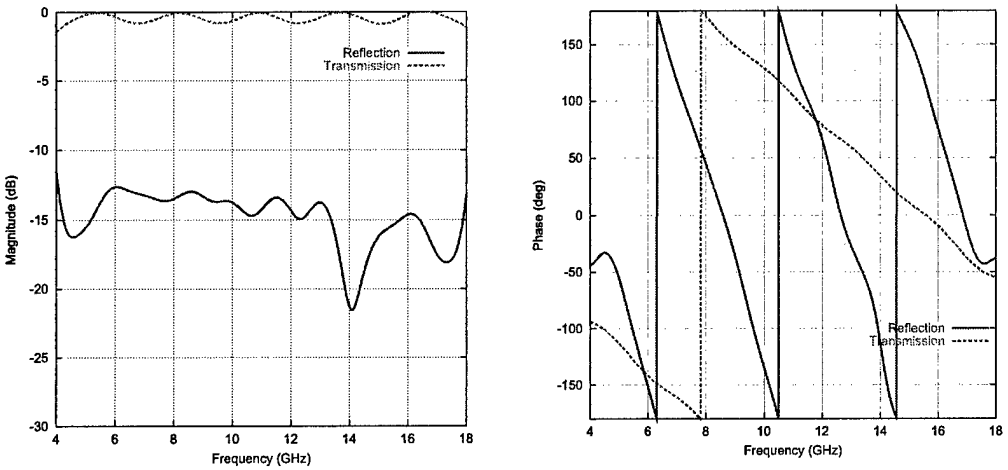

(a) Magnitude

(b) Phase

Figure 22: Measured reflection and transmission coefficient magnitudes and phases for a 1.0" thick sample of dry sand.

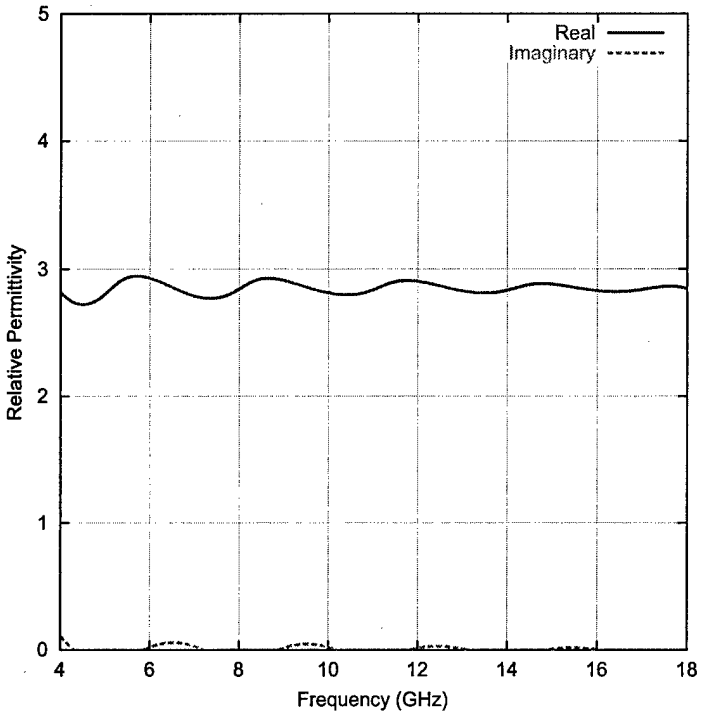

Figure 23: Complex permittivity for dry sand extracted from measured data.

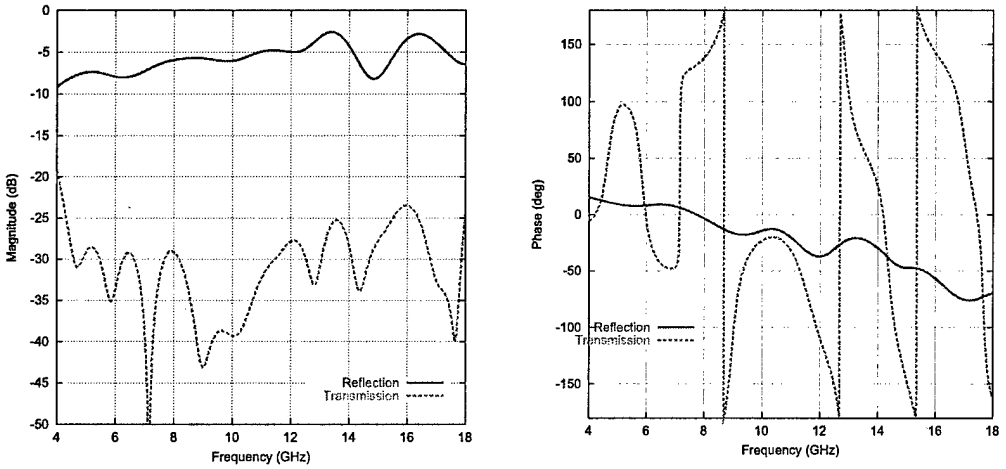

(a) Magnitude

(b) Phase

Figure 24: Measured reflection and transmission coefficient magnitudes and phases for a single 3-tab asphalt roof shingle.

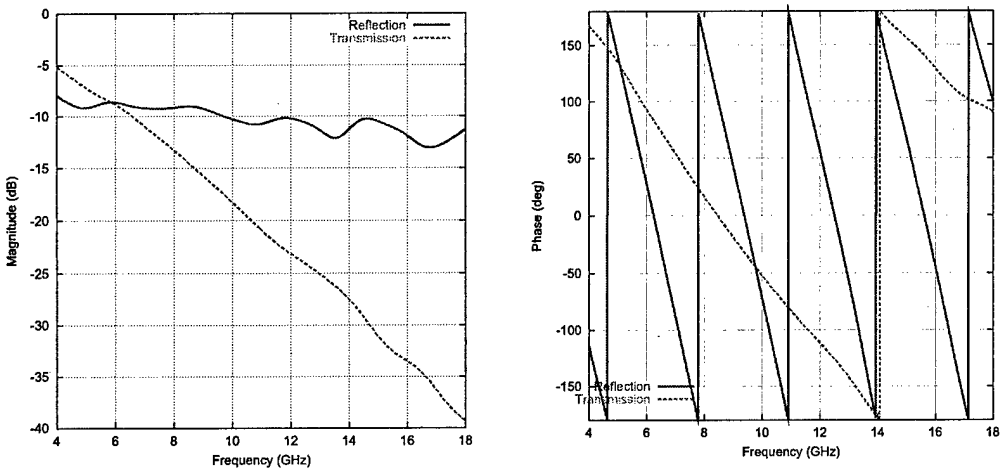

(a) Magnitude

(b) Phase

Figure 25: Measured reflection and transmission coefficient magnitudes and phases for a 1.0" thick sample of top soil.

4 Conclusions

The matched filter/chirp excitation represents a novel solution to the general problem of directly determining the impulse response of an LTI system wholly in the time domain. We have shown that, mathematically, the method offers a minimum error solution (via the matched filter), and that in the discrete case the technique can be used to exactly recover the impulse response given an appropriate relation between pulse duration, sampling interval, and chirp rate. We showed that our magic number is related to the Zak space condition given by the authors in a subsequent report, and that both treatments fail the Nyquist sampling criteria if the carrier frequency is larger than zero.

While mathematically intriguing, the chirp solution suffers substantially under practical implementations. By far the largest hurdle is the difficulty associated with synthesizing a complex chirp waveform, whose additive property is the crux of the closed-form integral equation solution. We showed through measurements of a host of materials of military interest that over narrow frequency ranges many of the materials have similar reflection coefficients that can only be resolved with wideband data. Unfortunately, the chirp pulse solution is not amenable to wide bandwidth pulses, as the chirp duration times and associate data collections become prohibitively large. This fact coupled with the high dynamic range achievable with frequency domain methods (through well-established heterodyne mixing) indicates that in practice the chirp waveform technique does not offer benefits that exceed traditional frequency domain material measurements.

References

[1] R. Tolimieri, "Multispectral SAR Imaging for Material Identification," Final Report AFRL-HE-BR-TR-2002-0125, June 2002.

[2] W. Davenport and W. Root, *An Introduction to the Theory of Random Signals and Noise,* pp 244 - 246.

[3] R. Tolimieri and M. An, "MISAR: Waveform Design and Filtering in Zak Space," Progress Report for Contract # FA9550-04-C-0003, 23 January 2004.